Phase transitions and critical phenomena in the two-dimensional Ising model with dipole interactions: A short-time dynamics study

C. M. Horowitz, M. A. Bab, M. Mazzini, M. L. Rubio Puzzo, and G. P. Saracco
Instituto de Investigaciones Fisicoquímicas Teóricas y Aplicadas (INIFTA), UNLP, CCT La Plata-CONICET, c.c. 16, Suc. 4, (1900) La Plata, Argentina
(Received 30 June 2015; published 12 October 2015)

The ferromagnetic Ising model with antiferromagnetic dipole interactions is investigated by means of Monte Carlo simulations, focusing on the characterization of the phase transitions between the tetragonal liquid and stripe of width h phases. The dynamic evolution of the physical observables is analyzed within the short-time regime for $0.5 \leqslant \delta \leqslant 1.3$, where δ is the ratio between the short-range exchange and the long-range dipole interaction constants. The obtained results for the interval $0.5 \leqslant \delta \leqslant 1.2$ indicate that the phase transition line between the $h = 1$ stripe and tetragonal liquid phases is continuous. This finding contributes to clarifying the controversy about the order of this transition. This controversy arises from the difficulties introduced in the simulations due to the presence of long-range dipole interactions, such as an important increase in the simulation times that limits the system size used, strong finite size effects, as well as to the existence of multiple metastable states at low temperatures. The study of the short-time dynamics of the model allows us to avoid these hindrances. Moreover, due to the fact that the finite-size effects do not significantly affect the power-law behavior exhibited in the observables within the short-time regime, the results could be attributed to those corresponding to the thermodynamic limit. As a consequence of this, a careful characterization of the critical behavior for the whole transition line is performed by giving the complete set of critical exponents.

DOI: 10.1103/PhysRevE.92.042127 PACS number(s): 64.60.−i, 75.70.Kw, 75.40.Cx

I. INTRODUCTION

In the last few decades, the study of thin magnetic films has attracted the attention of the scientific community. Part of this interest is motivated by their potential technological applications in many branches of science, such as catalysis [1], biotechnology [2,3], and magnetic recording media [4–7], among many others. From the theoretical point of view, these systems can be described by simple models that allow us to understand the interplay between the microscopic interactions and the macroscopic properties of magnetic materials. The thickness of the film plays a crucial role in its magnetic behavior; in particular, extremely thin films (of only a few monolayers) present magnetic moments that tend to align perpendicularly to the plane defined by the film. In this context, one of the most simple and widely studied model that describes the main properties of ultrathin magnetic films, in the strong anisotropy limit, is the two-dimensional Ising model with short-range ferromagnetic exchange and long-range antiferromagnetic dipole interactions. The dimensionless Hamiltonian is written as

$$\mathcal{H} = -\delta \sum_{\langle i;j \rangle} \sigma_i \sigma_j + \sum_{i<j} \frac{\sigma_i \sigma_j}{r_{ij}^3}, \qquad (1)$$

where $\sigma_i = \pm 1$ is the Ising spin variable oriented perpendicularly to the square lattice of size L, and $\delta = J/g$ is the ratio between the short-range exchange ($J > 0$) and the long-range dipole ($g > 0$) constants. Also, the first sum runs over all pairs of nearest-neighbor (NN) spins, while the second one runs over all pairs of spins (i, j) of the lattice separated by a distance r_{ij}, measured in crystal units. The energy is measured in units of g. In this model, the usual ferromagnetic order is destroyed by the frustration originated by the presence of dipole interactions. This fact results in a complex and interesting phase diagram (see Refs. [8–12]), which contributes to explaining a variety of experimentally observed structures, such as stripe domain patterns [13–16].

An important theoretical effort has been made in order to define the ground state of Hamiltonian (1) as a function of strength parameter δ [12,17–19]. MacIsaac and coauthors have shown that for $\delta < 0.425$ the ground state is antiferromagnetic (AF), while for $\delta > 0.425$ it is composed of a sequence of alternating stripes with opposite magnetization. These stripes are characterized by a constant width h, whose value increases with δ. By using Monte Carlo (MC) simulations on square lattice, it was possible to access the phase diagram in the plane $T - \delta$, where T is the temperature of the thermal bath [8–11,17,20]. For the case of pure dipole interactions ($\delta = 0$), the system presents a continuous phase transition at $T = 1.2$ (where T is given in units of g/k_B, with k_B being the Boltzmann constant) between the AF phase and a phase with broken orientational order, called the tetragonal liquid (TL) phase. It was found that the estimated critical exponents belonged to the two-dimensional Ising model universality class [8]. The TL phase is a disordered state characterized by a fourfold discrete rotational symmetry [21]. At low temperatures, the model still presents AF configurations in the range $0 < \delta < 0.4152$. The AF phase changes to irregular checkerboard configurations (IRC) with rectangular spin domains, observed in the narrow range $0.4152 < \delta < 0.4403$ [20]. For larger values of δ, the system state changes to spin stripe configurations, whose width h increases with δ. All transitions between the mentioned ordered phases have a first-order character [10,22,23]. In particular, the IRC $\rightarrow h = 1$ and the $h = 1 \rightarrow h = 2$ phase transitions occur at $\delta = 0.4403$ and $\delta = 1.2585$, respectively [8]. At higher temperatures, all the above-described ordered phases present a phase transition to the TL phase, except for narrow windows around some specific values of δ where an intermediate nematic phase, between the stripe and the tetragonal liquid ones, is observed [10,11]. The nematic phase is characterized by long-range orientational order but no long-range positional order. It is important to mention that, with a further temperature increase, the tetragonal fourfold

symmetry is continuously replaced by the full-rotational symmetry corresponding to the paramagnetic phase [13].

Despite progress in understanding the phase diagram because of the above-mentioned work, some details are still under discussion. In particular, controversial results about the order of the transitions between the stripe-tetragonal phases are found in the literature. In fact, a line of continuous phase transitions for $\delta \leqslant 2$ was reported [22], but in latter work [24] it was claimed that this line is first-order in the range $1 \leqslant \delta \leqslant 3$. On the other hand, Rastelli *et al.* [8,20] have found that for $\delta = 0.85$ the transition seems to be continuous, while closer to $\delta = 1.2585$ the transition is of first order. The authors have also given evidence that the transition keeps the first-order character for $\delta = 1.7$ and 2.5, but for larger values of δ their results were not conclusive. Pighín and Cannas [10] have calculated in detail the phase diagram in the region $0 < \delta < 4.2$, through both mean-field calculations and MC simulations. Their numerical results indicated that for $\delta = 1$ the system presents a weak first-order phase transition and a first-order one for larger δ. Since at $\delta = 1$ the phase transition seems to be first-order, the authors conjectured that a tricritical point must be present somewhere between $\delta = 0.85$ and $\delta = 1$. More recently, Fonseca *et al.* [9] have extensively investigated the phase diagram in the region $0.85 \leqslant \delta \leqslant 1.3$ by analyzing the complex partition function zeros from multicanonical algorithms. Their results supported the idea of a continuous phase transition line that ends in a tricritical point at $\delta = 1.2585$ (whose temperature is not well determined), from where a first-order phase transition takes place. Rizzi and Alves [11,25] have studied the case $\delta = 2$, and even though they applied reweighting techniques with multiple histograms, the presence of dipole interactions introduced strong finite-size effects that hinder the identification of the character of the phase transitions.

The discrepancies in the MC results described above are a consequence of the difficulties introduced by the long-range character of the dipole interaction. In fact, the long-range iterations imply that every spin directly feels the influence of the remaining spins of the system and its boundaries. The former produces an important increase in the CPU time that limits the system size used in the simulation, and the latter leads to strong finite-size effects. So any convincing finite-size effect scaling, together with a reliable determination of the critical exponents, becomes a difficult task to perform. Moreover, the existence of multiple metastable states at low temperature requires very long-time MC simulations in order to reach the equilibrium state, and the weak first-order character suggested for some $\delta's$ hinders its distinction from a continuous transition.

In this context, the short-time dynamics (STD), initially introduced by Janssen *et al.* [26], is a powerful technique to study the phase transitions by means of Monte Carlo simulations which has been applied to both equilibrium and nonequilibrium systems (see the reviews [27,28] and references therein). In fact, the STD method allows us to obtain both the critical point and the critical exponents of the model in the case of continuous phase transitions, or the metastability limits (spinodals points) in the case of first-order transitions in the thermodynamic limit, whichever the case is. Furthermore, due to its sensibility, STD has been successfully applied to differentiate a weak first-order phase transition from a continuous one [28,29]. For models with long-range interactions that decay algebraically with the distance between spins, the validity of this technique was proven theoretically [30,31] and numerically [29,32,33]. Due to the fact that STD studies are performed on the early evolution of the relevant observables, such as the order parameter and its moments or cumulants, the computational time is notably reduced, and this allows us to study larger system sizes.

In this work, the Ising model with dipole interactions is studied by means of short-time dynamics. In particular, the phase transition between tetragonal-liquid and stripe phases is characterized as a function of δ for $0.5 \leqslant \delta \leqslant 1.3$. The paper is organized as follows: in Sec. II the simulation details and a summary of STD technique are detailed, in Sec. III the results are presented, and our conclusions are reported in Sec. IV.

II. SHORT-TIME DYNAMICS AND SIMULATION DETAILS

In this section a brief summary of the STD method used in the characterization of phase transitions is given. Due to the fact that all phases present in the $T - \delta$ phase diagram of the Ising model with dipolar interactions have the magnetization equal to zero, it is necessary to define an order parameter sensitive to the change in the orientational order, such as the one introduced by Booth *et al.* [21]:

$$O_{hv} \equiv \frac{n_v - n_h}{n_v + n_h}, \tag{2}$$

where n_v (n_h) are the number of vertical (horizontal) bonds of the NN antiparallel spins. This definition ensures that $O_{hv} = +1$ (-1) when the system is in the stripe horizontal (vertical) phase, and $O_{hv} = 0$ in the tetragonal or paramagnetic phases. Also, the susceptibility (χ), the logarithmic derivative of the order parameter with respect to the reduced temperature evaluated at the critical point T_c (D), and the second order Binder cumulant (U) are defined as

$$\chi = \frac{1}{N}\left(\langle O_{hv}^2\rangle - \langle O_{hv}\rangle^2\right), \tag{3}$$

$$U = 1 - \frac{\langle O_{hv}^2\rangle}{\langle O_{hv}\rangle^2}, \tag{4}$$

$$D \equiv \left.\frac{\partial \log\langle O_{hv}\rangle}{\partial \tau}\right|_{\tau=0}, \tag{5}$$

where $\tau = (T - T_c)/T_c$ is the reduced temperature, $N = L^2$ and $\langle\cdots\rangle$ indicates the average performed over different samples with equivalent initial conditions. Hereafter, $\langle O_{hv}\rangle$ and $\langle O_{hv}^2\rangle$ will be referred to as O_{hv} and O_{hv}^2, respectively.

The main idea of STD is to analyze the time series of the above observables when the system is initialized with configurations that correspond to trivial fixed points [28]. In the present case, the fixed points correspond to the ground state ($T = 0$) and the paramagnetic one ($T = \infty$). In the case of a continous phase transition, it is expected that at early times of the dynamic evolution, these observables will exhibit a power-law behavior at the critical point, with exponents that are related to the usual critical exponents of the phase transition. For values of the control parameter $T \neq T_c$, but

within the critical region, the power law is modified by a scaling function. This fact can be used to determine the critical temperature as well as the critical exponents from the localization of the best power law (for more details see the review [28] and references therein).

For the case of the stripe-ordered initial condition corresponding to $T = 0$, the ansätze of the time evolution of the observables are the following:

$$O_{hv}(t) \propto t^{-\beta/\nu z}, \tag{6}$$

$$U(t) \propto t^{d/z}, \tag{7}$$

$$D(t) \propto t^{1/\nu z}, \tag{8}$$

$$\chi(t) \propto t^{\gamma/\nu z}, \tag{9}$$

where β, ν, and γ are the static exponents for the order parameter, correlation length, and susceptibility, respectively, and z the dynamic exponent for the time evolution of the correlation length.

However, if the system is started from paramagnetic-disordered initial conditions corresponding to $T = \infty$, the proposed scaling law is

$$O_{hv}^2(t) = \chi(t) \propto t^{\gamma/\nu z}. \tag{10}$$

By following the STD, the universal evolution is strictly valid in a well-defined time interval $(t_{\rm mic}, t_{\rm max})$, where $t_{\rm mic}$ and $t_{\rm max}$ are set when the correlation length $(\xi(t))$ is on the order of a single lattice spacing and the lattice size (L), respectively. Furthermore, $t_{\rm max}$ is very small in comparison with the time necessary for equilibration, so STD is free of the critical slowing down. For short-range models, the STD analysis is also free of finite-size effects since $\xi(t)$ remains smaller than L. For the case of long-range models this is no longer valid, and it was demonstrated that if a cutoff is introduced in the interaction sum, when periodic boundary conditions are implemented, it affects the validity range of the power law, but not the calculation of the critical exponents [32].

On the other hand, STD can also be applied to determine the metastability limits of the phases that coexist in a first-order phase transition [29]. In the case of long-range interaction models, metastability limits are identified as the spinodals. At these points, the susceptibility and relaxation times diverge, as in the case of a continuous phase transition, which allows us to define them as pseudocritical. In this way, for the stripe-ordered initial condition:

$$O_{hv}(t) \propto t^{\omega} + O_{hv}^{sp}, \tag{11}$$

where ω is an exponent and O_{hv}^{sp} is the value of the order parameter at the spinodal $(T_{\rm up})$. Also, the susceptibility diverges as a power law given by

$$\chi(t) \propto t^{\Omega}, \tag{12}$$

where Ω is an exponent. For the paramagnetic initial condition:

$$O_{hv}(t)^2 \propto t^{\omega^*}, \tag{13}$$

where ω^* is another exponent, and $O_{hv}^{sp} = 0$ at the spinodal $(T_{\rm down})$. The difference $T_{\rm up} - T_{\rm down}$ is a measure of the strength of the transition, and it allows us to distinguish between a continuous [where $T_{\rm up} = T_{\rm down} = T_c$, Eqs. (11) and (13) become Eqs. (6) and (10), respectively] and a weak first-order transition ($T_{\rm down} < T_{\rm trans} < T_{\rm up}$, where $T_{\rm trans}$ is the transition temperature) [28].

In order to reduce the finite size effects due to the mentioned cutoff, in the present paper periodic boundary conditions were implemented by tiling the entire space with replicas of the original finite system [34]. The combination of the original system and all of its replicas (hereafter the aggregation) can be represented for a square lattice by a pair (L,m) of integers, where m is the size of the aggregation in units of replicas.

According to the periodicity of the aggregation $\sigma_i \equiv \sigma(\mathbf{r}_i) = \sigma(\mathbf{R} + \mathbf{r}_i)$ (where $\mathbf{R}$ is the translation from the original system to any of the replicas), the second term on the right-hand side of Eq. (1) can be written as

$$\sum_{i<j} \frac{\sigma_i \sigma_j}{r_{ij}^3} = \sum_{i \leqslant j} \sum_{\mathbf{R}} A(\mathbf{r}_i, \mathbf{R} + \mathbf{r}_j) \sigma(\mathbf{r}_i) \sigma(\mathbf{r}_j). \tag{14}$$

The function A is related to the dipole interaction between a pair of spins in the aggregation, and it has to take into account the interaction between a spin and its own copies in the replicated systems, but it must exclude the nonphysical interaction of a spin with itself. In this way, A could be defined as

$$A(\mathbf{r}_i, \mathbf{R} + \mathbf{r}_j) = \begin{cases} 0 & \text{if } i = j, \text{ and } \mathbf{R} = \mathbf{0}, \\ |\mathbf{r}_i - \mathbf{R} - \mathbf{r}_j|^{-3} & \text{otherwise.} \end{cases} \tag{15}$$

The sum over all replicas depends only on i and j, but not on the orientation of the spins, so it can be calculated in advance. This fact reduces the Hamiltonian to the general Ising model Hamiltonian with effective interaction coefficients:

$$\mathcal{H} = \sum_{i \leqslant j} J_{ij}^{\rm eff} \sigma(\mathbf{r}_i) \sigma(\mathbf{r}_j), \tag{16}$$

where

$$J_{ij}^{\rm eff} = \begin{cases} -\delta + \sum_{\mathbf{R}} A(\mathbf{r}_i, \mathbf{R} + \mathbf{r}_j), & \text{if } i \text{ and } j \text{ are NN,} \\ \sum_{\mathbf{R}} A(\mathbf{r}_i, \mathbf{R} + \mathbf{r}_j) & \text{otherwise.} \end{cases} \tag{17}$$

The accuracy of $\sum_{\mathbf{R}} A(\mathbf{r}_i, \mathbf{R} + \mathbf{r}_j)$ depends on the size of the aggregation (m) and its implementation by using a parallel code is straightforward, so m can be chosen quite large. Also, as only relative positions matter, it is obvious that not all of the $N(N+1)/2$ coefficients in a system with N spins will be different; actually there are about $\sim(L/2+1)(L/2+2)/2$. Furthermore, if the time unit in Monte Carlo simulations is defined as N attempts to flip a spin, then the time required to perform a Monte Carlo step (MCS) for an (L,m) aggregation depends only on the number of spins N of the original system.

The method described above is an alternative to the Ewald summation techniques [35]. For the present model, the described method works very well since the dipole term decreases as r^{-3} and the series in Eq. (17) is rapidly convergent. It is worth mentioning that we have checked this method and verified that $m \sim 5000$ is enough to reproduce the results reported by other authors.

III. RESULTS AND DISCUSSION

Monte Carlo simulations were performed by using heat-bath dynamics in a square lattice of size $L = 128$ with periodic boundary conditions (aggregation size $m = 5000$). The STD observables were measured up to 5000 MCS and averaged over $n_s = 3000$ different realizations.

In order to determine the number of independent realizations n_s as well as the error bars, a variant of the blocking method [36] was used. In this way, the time dependence of each observable is fitted, and it is checked that the error that emerges from the fit verifies the following condition: if the fit is repeated for several independent sets of measurements, the obtained values spread within the proposed error. This procedure becomes stable for $n_s \geqslant 3000$.

Figure 1(a) shows the time evolution of the order parameter for $\delta = 1.2$ when the system is annealed from the ground-state ordered configuration (OC), i.e., from the $h = 1$ phase. As can be seen, a power-law behavior is observed near $T = 0.30975$. In order to study a possible critical regime, the temperature range was set at those temperatures that exhibit small deviations from a power-law behavior. From the study of the logarithmic derivative of O_{hv} with respect to the logarithm of time, $d_1(t) \equiv \partial[\ln O_{hv}(t)]/\partial \ln t$, the critical or pseudocritical regime was identified to be in the interval $0.309 < T < 0.311$ [$T = 0.309$ and $T = 0.311$ present evident deviations from the power-law behavior; see inset of Fig. 1(a)]. This study yields the best power-law behavior at $T = 0.30975(25)$, where the error bars were assessed by considering the closest curves that present the smallest deviations. Furthermore, the data corresponding to $T = 0.30975$ (shown in the inset) allow us to determine the times t_{mic} and t_{max} at $t \approx 150MCS$ and $t > 5000MCS$, respectively.

Figure 1(b) displays the second moment of the order parameter O^2_{hv} as a function of time when the system is quenched from the high-temperature paramagnetic phase, corresponding to disordered configurations at $T = \infty$ (DCs). In this case, the critical or pseudocritical regime was identified to be within the interval $0.308 < T < 0.312$, as can be observed in the inset of Fig. 1(b), where $d_2(t) \equiv \partial[\ln O^2_{hv}(t)]/\partial \ln t$ is shown ($T = 0.308$ and $T = 0.312$ present evident deviations from the power-law behavior). The best power-law behavior was obtained at $T = 0.310(1)$, where the error bars were estimated in the same way as in the previous case. Here the validity range of the STD power law was determined from $d_2(t)$, and it is similar to that of the OC case.

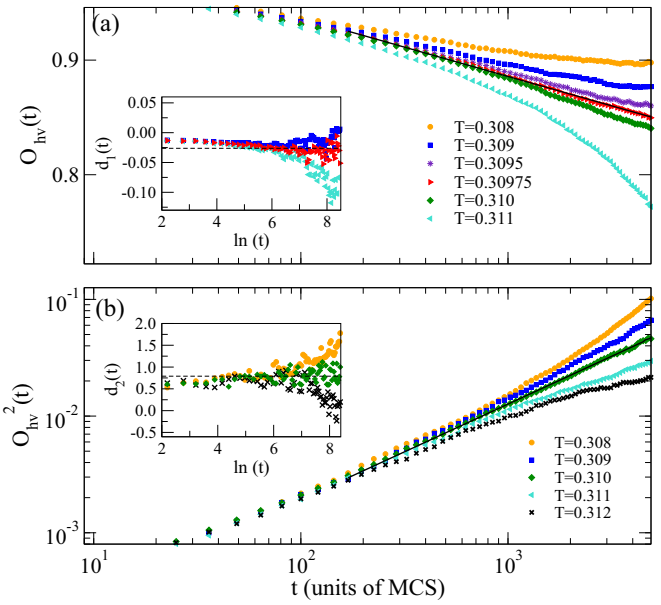

FIG. 1. (Color online) Log-log plot of the time evolution of: (a) order parameter $O_{hv}(t)$ at the temperatures from top to bottom: $T = 0.308$, $T = 0.309$, $T = 0.3095$, $T = 0.30975$, $T = 0.310$, and $T = 0.311$ when the system was initialized from OC; and (b) second moment of the order parameter O^2_{hv} at the temperatures from top to bottom $T = 0.308$, $T = 0.309$, $T = 0.310$, $T = 0.311$, and $T = 0.312$ when the system was initialized from DC. The best fits to Eqs. (6) and (10) correspond to the temperatures $T = 0.30975$ (OC) and $T = 0.310$ (DC), respectively. They are shown with solid lines. Insets of figures (a) and (b) show $d_1(t) \equiv \partial[\ln O_{hv}(t)]/\partial \ln t$ and $d_2(t) \equiv \partial[\ln O^2_{hv}(t)]/\partial \ln t$ as a function of the logarithm of time, respectively. The data correspond to $\delta = 1.2$ and $L = 128$. More details in the text.

The described results indicate that $T = 0.30975(25)$ and $T = 0.310(1)$ are the temperatures where O_{hv} and O^2_{hv} fit Eqs. (6) and (10), respectively. Both values of T coincide, within error bars, which suggests that the phase transition is continuous, and they represent the critical temperature (T_c). The error in the above-reported value of T for the case of the DC initial configurations is influenced by less sensitivity to the temperature variation of the O^2_{hv}. As a result, the corresponding error bars are larger than those reported for the OC case. From the fit of the data corresponding to the OC (DC) initial

TABLE I. Critical temperatures and dynamic exponents obtained from the STD analysis. The data correspond to initial configurations OC and DC. More details in the text.

δ	T_c (OC)	T_c (DC)	$\gamma/(\nu z)$ (DC)	$\gamma/(\nu z)$ (OC)	d/z (OC)	$1/(\nu z)$ (OC)	$\beta/(\nu z)$ (OC)
0.5	0.2890(5)	0.289(1)	0835(2)	0.799(9)	0.913(5)	0.665(5)	0.0632(6)
0.6	0.3625(5)	0.363(1)	0.770(3)	0.755(8)	0.938(6)	0.610(5)	0.0922(3)
0.7	0.397(1)	0.398(2)	0.757(7)	0.745(7)	0.962(5)	0.557(4)	0.1043(4)
0.8	0.4115(5)	0.412(1)	0.730(5)	0.741(5)	0.968(6)	0.545(6)	0.1138(2)
0.9	0.4110(5)	0.411(1)	0.724(5)	0.728(8)	0.928(8)	0.535(6)	0.1062(3)
1.0	0.395(1)	0.396(2)	0.747(5)	0.740(8)	0.903(8)	0.552(6)	0.0804(5)
1.1	0.364(1)	0.365(2)	0.763(5)	0.754(8)	0.863(8)	0.623(3)	0.0542(2)
1.2	0.30975(25)	0.310(1)	0.790(3)	0.773(8)	0.812(6)	0.712(6)	0.0262(2)
1.3	0.3305(5)	0.326(1)	–	–	–	–	–

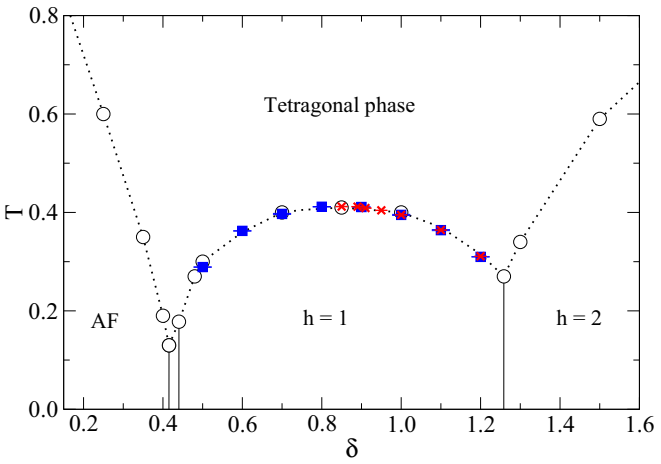

FIG. 2. (Color online) Phase diagram in the plane $T - \delta$ for $\delta \leqslant 1.6$. Open circles and crosses were taken from Refs. [8] and [9], respectively; the squares correspond to data obtained in the present work. Dotted lines are to guide the eye; solid lines represent the first-order phase transitions. For more details, see the introduction.

condition by using Eq. (6) [Eq. (10)], the STD exponent $\beta/\nu z$ ($\gamma/\nu z$) was determined, and it is reported in Table I.

This methodology was applied for different values of δ in the range $0.5 \leqslant \delta \leqslant 1.20$. The obtained results are listed in Table I and shown in Fig. 2. For all studied values of δ, the critical temperatures determined from both initial conditions are the same, within error bars. This fact indicates that the phase transition between TL and $h = 1$ phases is a continuous phase transition line. In addition, Fig. 2 shows that the present results are in excellent agreement with those obtained by Rastelli *et al.* [8] and by Fonseca *et al.* [9].

In order to determine the critical exponents as a function of δ, the time evolution at the critical point of the Binder cumulant, $U(t)$, the logarithmic derivative of O_{hv} with respect to the reduced temperature, $D(t)$, and the susceptibility, $\chi(t)$, were measured. In particular, the data corresponding to $\delta = 1.2$ are shown in Fig. 3. The fits according to Eqs. (7), (8), and (9) are shown with solid lines in Figs. 3(a), 3(b), and 3(c), respectively. So the STD exponents were determined from these fits. This procedure was applied to all the investigated values of δ, and the obtained exponents are reported in both Table I and Fig. 4. As can be observed, there is a good agreement, within error bars, between the values of $\gamma/\nu z$ obtained for both initial conditions (OC and DC). The largest difference was found for $\delta = 0.5$, and it is less than 5%. This fact supports the idea of a continuous character of the phase transition line between $h = 1$ and TL phases.

By combining the STD exponents, the critical exponents were calculated as a function of δ (see Table II). Figure 5 shows the exponents β, γ, ν, z as well as the ratio γ/ν, which were determined from OC initial condition. Figure 5(b) also presents the exponent γ/ν estimated by using $\gamma/\nu z$ and z corresponding to DC and OC initial conditions, respectively. Both determinations of γ/ν are in good agreement, and the differences are at most 5% (for $\delta = 0.5$). The exponents ν and γ/ν, recently reported by Fonseca *et al.* [9] for the range $0.85 \leqslant \delta \leqslant 1.2$, are also included in Fig. 5 and Table II for the sake of comparison. As can be observed in Fig. 5, all

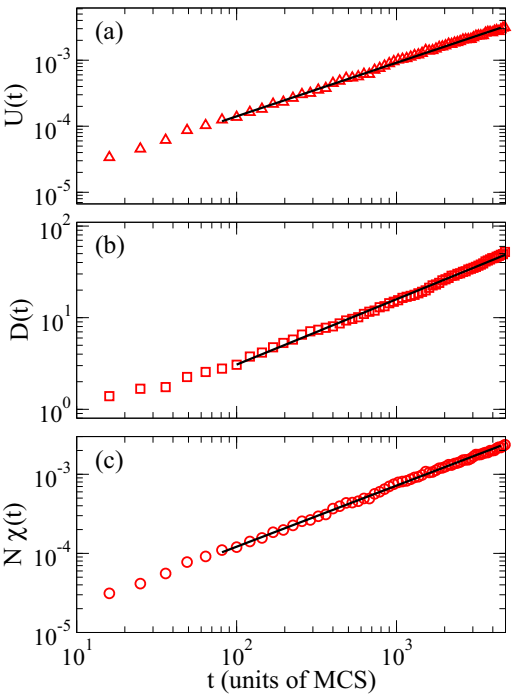

FIG. 3. (Color online) Log-log plot of the observables (a) $U(t)$, (b) $D(t)$, and (c) $N\chi(t)$ versus time, when the system is initialized from OC, for $\delta = 1.2$, $L = 128$, $T_c = 0.30975$. The solid lines correspond to the fit of data with Eqs. (7), (8), and (9) for $U(t)$, $D(t)$ and $\chi(t)$, respectively. More details in the text.

the reported results are in good agreement, within error bars. It is worth mentioning that, to the best of our knowledge, this is the first time the dynamic critical exponent (z) for the range $0.5 \leqslant \delta \leqslant 1.2$ and the static ones (β, γ, ν) for the range $0.5 \leqslant \delta \leqslant 0.8$ have been estimated. In addition, the obtained exponents ν and γ/ν in the range $1.1 \leqslant \delta \leqslant 1.2$ are closed to those determined by Jin *et al.* [37,38] for the multicritical point of the short-range J_1-J_2 Ising model where J_1 and J_2

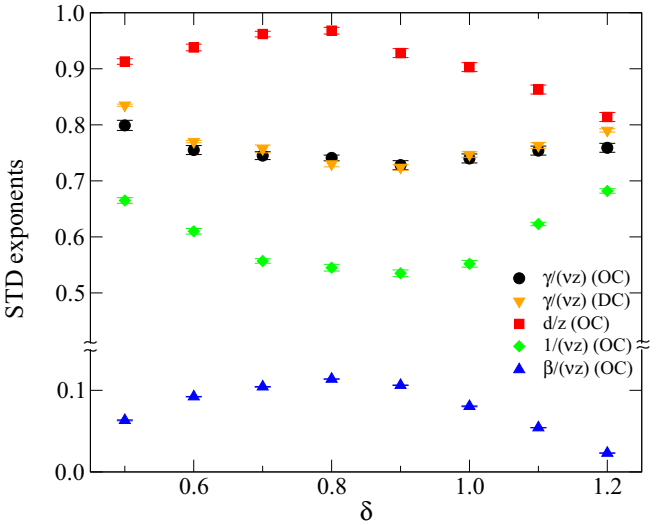

FIG. 4. (Color online) STD critical exponents versus δ obtained for both initial conditions (OC and DC) as is indicated. More details in the text.

TABLE II. Critical exponents calculated from STD ones corresponding to the continuous phase transition line between the TL and $h = 1$ phases. Here (DC/OC) indicates that the exponent was obtained by combining the exponents $\gamma/\nu z$ and z corresponding to DC and OC initial conditions in the STD. The table also includes the values that were taken from Ref. [9].

δ	β	γ	z	ν	ν [9]	γ/ν	γ/ν(DC/OC)	γ/ν [9]
0.5	0.095(1)	1.20(2)	2.19(1)	0.686(7)	ND	1.75(3)	1.83(1)	ND
0.6	0.151(14)	1.24(2)	2.13(1)	0.769(8)	ND	1.61(3)	1.64(3)	ND
0.7	0.187(15)	1.34(2)	2.08(1)	0.864(8)	ND	1.55(2)	1.57(2)	ND
0.8	0.209(2)	1.36(2)	2.07(1)	0.89(1)	ND	1.53(3)	1.51(2)	ND
0.9	0.199(2)	1.36(2)	2.13(2)	0.88(1)	ND	1.55(3)	1.54(3)	ND
1.0	0.146(2)	1.34(2)	2.21(2)	0.82(1)	0.83(2)	1.64(3)	1.65(3)	1.59(2)
1.1	0.0870(5)	1.21(1)	2.32(2)	0.693(7)	0.708(13)	1.75(3)	1.77(2)	1.736(21)
1.2	0.0368(4)	1.09(1)	2.46(2)	0.570(6)	0.61(1)	1.90(1)	1.95(2)	1.99(3)

are the ferromagnetic first-neighbor and antiferromagnetic second-neighbor exchanges, respectively. The J_1-J_2 Ising model presents a line of continuous phase transitions between a stripes $h = 1$ and paramagnetic phases that belongs to the Ashkin-Teller universality class. The continuous line ends at $|J_1|/J_2 \simeq 1.49$, where the critical exponents are $\nu = 2/3$ and $\gamma/\nu = 7/4$, and changes to a first-order one. This could indicate a possible connection between the model studied in the present work and the J_1-J_2 model that deserves more careful research.

Let us consider $\delta = 1.3$ that belongs to the $h = 2$-TL phase transition region. The dynamic behavior of the order parameter O_{hv} when the system is started from OC initial configuration ($h = 2$) shown in Fig. 6(a) evidences metastability effects, i.e., $O_{hv}^{sp} \neq 0$ [see Eq. (11)]. In order to determine the spinodal temperature ($T_{\rm up}$), the susceptibility was measured at different temperatures, and it is shown in the inset of Fig. 6(a). The best fit of the data to Eq. (12), shown as a solid line, was obtained for $T = 0.3305$. In this way, $T_{\rm up} = 0.3305(5)$ where the error bars were determined as in previous cases. This result allows us to estimate the value of $O_{hv}^{sp} = 0.89(1)$ by fitting the data with Eq. (11) [see Fig. 6(a)]. On the other hand, when the system is started from DC configurations, the best power-law behavior of O_{hv}^2, given by Eq. (13), is observed for $T = 0.326(1)$. This is shown in Fig. 6(b). In this way, this temperature can be associated with the tetragonal-spinodal point $T_{\rm down}$. The difference between the obtained spinodal temperatures, which are also reported in Table I, suggests a first-order phase transition with a weak character, in agreement with previous work [8–10].

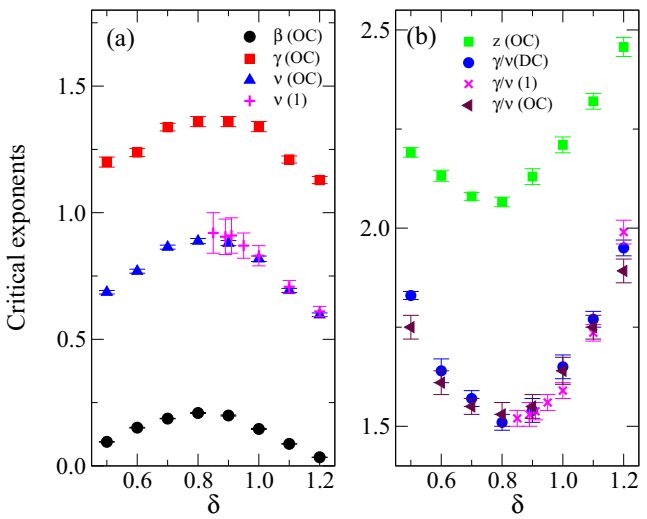

FIG. 5. (Color online) Critical exponents calculated from the STD ones corresponding to the OC: (a) β, γ, and ν, and (b) z and γ/ν. Panel (b) also includes the ratio γ/ν determined by using $\gamma/\nu z$ and z from DC and OC, respectively. The data (1) were extracted from Ref. [9] and are shown for the sake of comparison.

IV. CONCLUSIONS

In this work the ferromagnetic Ising model with antiferromagnetic dipole interactions was investigated by means of short-time dynamics (STD). Specifically, the order of the phase

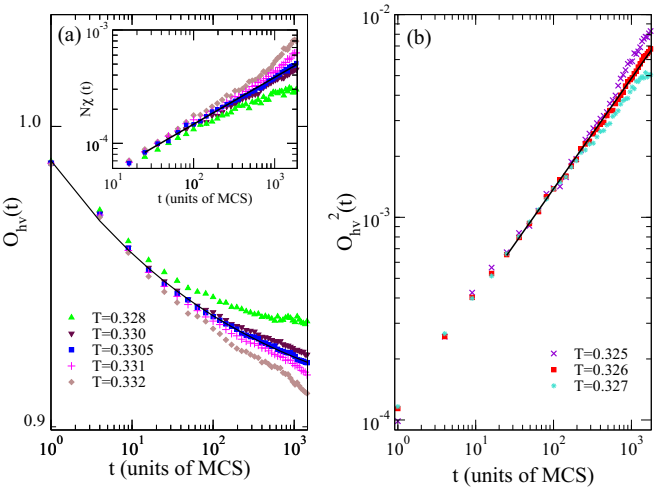

FIG. 6. (Color online) Log-log plot of the time evolution of (a) order parameter $O_{hv}(t)$ at the temperatures from top to bottom $T = 0.328$, $T = 0.330$, $T = 0.3305$, $T = 0.331$, and $T = 0.332$ when the system was initialized from OC and (b) second moment of the order parameter O_{hv}^2 at the temperatures from top to bottom $T = 0.325$, $T = 0.326$, and $T = 0.327$ when the system was initialized from DC. The best fits to Eqs. (11) and (13) correspond to the temperatures $T = 0.3305$ (OC) and $T = 0.326$ (DC), and they are shown with solid lines. The inset shows the susceptibility $\chi(t)$ for the indicated temperatures and the best fit to Eq. (12) obtained for $T = 0.3305$ (solid line). The data correspond to $\delta = 1.3$ and $L = 128$. More details in the text.

transitions between the tetragonal liquid (TL) and stripe of width h phases was analyzed in the interval $0.5 \leqslant \delta \leqslant 1.3$.

By initializing the system from ground-state (ordered) and paramagnetic (disordered) configurations, the time evolution of the STD observables was recorded. For the interval $0.5 \leqslant \delta \leqslant 1.2$, the expected power-law regimes were obtained at the same temperatures, within error bars, from both initial conditions. This fact indicates that the phase transition line between the $h = 1$ and TL phases is continuous. Moreover, the STD exponent obtained from the time evolution at the critical point of the susceptibility was found to be the same (within the error bars) in both initial conditions, supporting the continuous character. This result is in agreement with that reported by Fonseca *et al.* [9] by using the complex partition function zeros from multicanonical algorithms. For $\delta = 1.3$, the spinodal temperatures obtained from both initial conditions are slightly different. This fact suggests the existence of a weak first-order phase transition at this point, according to previous work [8–10].

It is important to stress that the continuous character of the phase transition line between $h = 1$ and TL phases obtained in this work contributes to clarify the controversy about the order of this transition in the region $0.85 \leqslant \delta \leqslant 1.2$. This statement is achieved by the advantages provided by the STD method that allows us to study this model without reaching equilibrium states for starting the measurements. This is a fundamental fact, since it avoids major difficulties that were present in previous work such as the critical slowing down, the existence of multiple metastable states at low temperatures, and strong finite size effects. Furthermore, since the latter do not significantly affect the power-law behavior exhibited in the observables within the short-time regime, our results could be attributed to those corresponding to the thermodynamic limit.

Moreover, the critical exponents β, γ, ν, and z corresponding to the transition line were obtained from the STD exponents. The values of ν and γ/ν obtained are in agreement with those estimated by Fonseca *et al.* [9] for the range $0.85 \leqslant \delta \leqslant 1.2$. It is important to mention that the exponents β, γ, and ν (in the interval $0.5 \leqslant \delta \leqslant 0.85$) and the dynamic exponent z (for $0.5 \leqslant \delta \leqslant 1.2$) are given here.

To summarize, the results reported in this work confirm the continuous character of the phase transition line between $h = 1$ and TL phases and give a complete characterization of the critical behavior in this line.

ACKNOWLEDGMENTS

This work was supported by CONICET and UNLP (Argentina). We thank UnCaFiQT (SNCAD) for computational resources. Very useful comments by S. A. Cannas are also acknowledged.

[1] R. Reeve, S. L. Chin, K. P. Kooper, A. Ionescu, and C. H. W. Barnes, Electron beam tuning of the magnetic anisotropy in Co/Cu(110) films, IEEE Trans. Magnetics **47**, 1554 (2011).

[2] T. J. Hayward, B. Hong, K. N. Vyas, J. J. Palfreyman, J. F. K. Cooper, Z. Jiang, J. R. Jeong, J. Llandro, T. Mitrelias, J. A. C. Bland, and C. H. W. Barnes, Magnetic micro-barcodes for molecular tagging applications, J. Phys. D **43**, 175001 (2010).

[3] C. Liang, C. P. Gooneratne, Q. X. Wang, Y. Liu, Y. Gianchandani, and J. Kosel, Magnetic properties of FeNi-based thin film materials with different additives, Biosensors **4**, 189 (2014).

[4] R. Lavrijsen, J. H. Lee, A. Fernández-Pacheco, D. C. M. C. Petit, R. Mansell, and R. P. Cowburn, Magnetic ratchet for three-dimensional spintronic memory and logic, Nature (London) **493**, 647 (2013).

[5] O. Hellwig, A. Berger, J. B. Kortright, and E. E. Fullerton, Domain structure and magnetization reversal of antiferromagnetically coupled perpendicular anisotropy film, J. Mag. Mag. Mat. **319**, 13 (2007).

[6] O. Hellwig, A. Berger, and E. E. Fullerton, Magnetic reversal and domain structure in perpendicular AF-coupled films, J. Mag. Mag. Mat. **290**, 1 (2005).

[7] Y. Shiroishi, K. Fukuda, I. Tagawa, S. Takenoiri, H. Tanaka, H. Mutoh, and N. Yoshicawa, Future options for HDD storage, IEEE Trans. Mag. **45**, 3816 (2009).

[8] E. Rastelli, S. Regina, and A. Tassi, Phase diagram of a square ising model with exchange and dipole interactions: Monte Carlo simulations, Phys. Rev. B **76**, 054438 (2007).

[9] J. S. M. Fonseca, L. G. Rizzi, and N. A. Alves, Stripe-tetragonal phase transition in the two-dimensional Ising model with dipole interactions: Partition function zeros approach, Phys. Rev. E **86**, 011103 (2012).

[10] S. A. Pighín and S. A. Cannas, Phase diagram of an Ising model for ultrathin magnetic films: Comparing mean field and Monte Carlo predictions, Phys. Rev. B **75**, 224433 (2007).

[11] L. G. Rizzi and N. A. Alves, Phase transitions and autocorrelation times in two-dimensional ising model with dipole interactions, Physica B **405**, 1571 (2010).

[12] A. Giuliani, J. L. Lebowitz, and E. H. Lieb, Checkerboards, stripes, and corner energies in spin models with competing interactions, Phys. Rev. B **84**, 064205 (2011).

[13] K. De'Bell, A. B. MacIsaac, and J. P. Whitehead, Dipolar effects in magnetic thin films and quasi-two-dimensional systems, Rev. Mod. Phys. **72**, 225 (2000).

[14] O. Portmann, A. Vaterlaus, and D. Pescia, An inverse transition of magnetic domain patterns in ultrathin films, Nature (London) **422**, 701 (2003).

[15] O. Portmann, A. Vaterlaus, and D. Pescia, Observation of Stripe Mobility in a Dipolar Frustrated Ferromagnet, Phys. Rev. Lett. **96**, 047212 (2006).

[16] N. Bergeard, S. Schaffert, V. López-Flores, N. Jaouen, J. Geilhufe, C. M. Günther, M. Schneider, C. Graves, T. Wang, B. Wu, A. Scherz, C. Baumier, R. Delaunay, F. Fortuna, M. Tortarolo, B. Tudu, O. Krupin, M. P. Minitti, J. Robinson, W. F. Schlotter, J. J. Turner, J. Lüning, S. Eisebitt, and C. Boeglin, Irreversible transformation of ferromagnetic ordered stripe domains in single-shot infrared-pump/resonant-x-ray-scattering-probe experiments, Phys. Rev. B **91**, 054416 (2015).

[17] A. B. MacIsaac, J. P. Whitehead, M. C. Robinson, and K. De'Bell, Striped phases in two-dimensional dipolar ferromagnets, Phys. Rev. B **51**, 16033 (1995).

[18] A. B. MacIsaac, J. P. Whitehead, K. De'Bell, and K. Sowmya Narayanan, Monte Carlo study of two-dimensional Ising dipolar antiferromagnets as a model for rare-earth ordering in the R-Ba-Cu-O compounds (R = rare earth), Phys. Rev. B **46**, 6387 (1992).

[19] M. B. Taylor and B. L. Gyorffy, A ferromagnetic monolayer with model spin-orbit and dipole-dipole interactions, J. Phys.: Condens. Matter **5**, 4527 (1993).

[20] E. Rastelli, S. Regina, and A. Tassi, Phase transitions in a square Ising model with exchange and dipole interactions, Phys. Rev. B **73**, 144418 (2006).

[21] I. Booth, A. B. MacIsaac, J. P. Whitehead, and K. De'Bell, Domain Structures in Ultrathin Magnetic Films, Phys. Rev. Lett. **75**, 950 (1995).

[22] P. M. Gleiser, F. A. Tamarit, and S. A. Cannas, Metastable states in a two-dimensional ising model with dipolar interactions, Physica D **168**, 73 (2002).

[23] P. M. Gleiser, F. A. Tamarit, S. A. Cannas, and M. A. Montemurro, Slow dynamics in a two-dimensional Ising model with competing interactions, Phys. Rev. B **68**, 134401 (2003).

[24] S. A. Cannas, D. A. Stariolo, and F. A. Tamarit, Stripe-tetragonal first-order phase transition in ultrathin magnetic films, Phys. Rev. B **69**, 092409 (2004).

[25] L. G. Rizzi and N. A. Alves, Multicanonical simulation and trapping due to high free-energy barriers in an Ising model for ultrathin magnetic films, J. Comput. Interdiscipl. Sci. **2**, 79 (2011).

[26] H. K. Janssen, B. Schaub, and B. Schmittmann, New universal short-time scaling behavior of critical relaxation processes, Z. Phys. B **73**, 539 (1989).

[27] B. Zheng, Monte Carlo simulations of short-time critical dynamics, Int. J. Modern Phys. B **12**, 1419 (1998).

[28] E. V. Albano, M. A. Bab, G. Baglietto, R. A. Borzi, T. S. Grigera, E. S. Loscar, D. E. Rodríguez, M. L. Rubio Puzzo, and G. P. Saracco, Study of phase transitions from short-time non-equilibrium behavior, Rep. Prog. Phys. **74**, 026501 (2011).

[29] T. S. Grigera, E. S. Loscar, E. E. Ferrero, and S. Cannas, Nonequilibrium characterization of spinodal points using short time dynamics, J. Chem. Phys. **131**, 024120 (2009).

[30] Y. Chen, Short-time dynamics of a random Ising model with long-range interaction, Phys. Rev. E **66**, 037104 (2002).

[31] Y. Chen, S. Guo, Z. Li, and A. Ye, Short-time behavior of the kinetic spherical model with long-ranged interactions, Eur. Phys. Rev. J. B **15**, 97 (2000).

[32] D. E. Rodriguez, M. A. Bab, and E. V. Albano, Study of the nonequilibrium critical quenching and the annealing dynamics for the long-range Ising model in one dimension, J. Stat. Mech.: Theory Exp. (2011) P09007.

[33] K. Uzelac, Z. Glumac, and O. S. Narisć, Short-time dynamics in the 1D long-range Potts model, Eur. Phys. J. B **63**, 101 (2008).

[34] R. Rüger and R. Valentí, Pattern formation in the dipolar Ising model on a two-dimensional honeycomb lattice, Phys. Rev. B **86**, 024431 (2012).

[35] P. P. Ewald, Die Berechnung optischer und elektrostatischer Gitterpotentiale, Ann. Phys. **369**, 253 (1921).

[36] M. E. J. Newman and G. T. Barkema, *Monte Carlo Methods in Statistical Physics* (Oxford University Press, Oxford, 1999).

[37] S. Jin, A. Sen, and A. W. Sandvik, Ashkin-Teller Criticality and Pseudo-First-Order Behavior in a Frustrated Ising Model on the Square Lattice, Phys. Rev. Lett. **108**, 045702 (2012).

[38] S. Jin, Arnab Sen, W. Guo, and A. W. Sandvik, Phase transitions in the frustrated Ising model on the square lattice, Phys. Rev. B **87**, 144406 (2013).